ENGINEERING RESEARCH JOURNAL (ERJ)
Vol. 1, No. 50 October 2021, pp.67-76
Journal Homepage: erj.bu.edu.eg

Experimental study and thermal performance evaluation of staggered cross flow heat exchangers of semi-circular tubes: I- Effect of pitch ratio and space between bases

A.A.Alghrubah, M.A. Abd Elrahman, M.F. Abd Rabbo, Y.A. Al-Mashad, M.R. Salem

Mechanical Engineering Department, Faculty of Engineering at Shoubra, Benha University, Shoubra, Cairo, Egypt

Abstract : Staggered cross flow heat exchangers are commonly employed as air coolers and steam generators. This study aims to boost their thermal performance by proposing a modification to the tube geometry; semicircular tube (SCT) instead of complete circular tube (CCT). Through the runs, numerous gaps between SCTs-bases with different pitches in both longitudinal/transversal directions are tested. The runs are performed with moving cooling water through the tubes while heating air flows across the tube bundles. The results state that the SCT can be used as a passive approach for augmenting the heat exchange rates. As geometry, increasing the gap between their bases increases both the heat exchange rate and fluid pressure loss at the same time. Additionally, reducing the longitudinal and/or transversal pitch ratios leads to enlarging these increases. In addition, the thermal performance index (*TPI*) is slightly augmented by extending the distance between the SCTs' bases or reducing the transversal and/or longitudinal spacings. Also, an increase in the *TPI* is resulted by raising the airflow rate. Moreover, the extreme determined *TPI* is 1.98.

Keywords: Staggered; Semi-circular; Bases' gap; Pitches; Performance.

1. Introduction

In furthermost of industries, heat is transported via heat exchangers as in the biochemical, electric power, refrigeration, heat recovery industries. Accordingly, augmenting the heat exchange above that in the usual or standard practice can significantly improve the thermal efficiency in such applications as well as the economics of their design and operation [1]. One of the main types of heat exchange approaches is bundles of tubes in cross flow. Their thermal attributes are very crucial to be analyzed [2, 3]. The history presents several woks on the hydrothermal behaviour of tube bundles. Via the pertinent data accessible, many investigators estimated a correlation to assess the heat loading rate through staggered CCT banks [4-9]. Biery [10] studied the heat exchange from a finned staggered CCT bank. Several configurations of the fins were applied. A growth in the hydrothermal performance was resulted. Merker and Hanke [11] performed laboratory tests on the heat exchange and pressure loss of a cross flow on staggered oval/CCT banks at different spacings. The results assured that the oval shape reduced the flow resistance. Kim et al. [12] dealt with plain finned staggered CCT bank. Correlations were established to assess the thermal performance attributes. Torii et al. [13] practically inspected the influence of conducting vortex generators to finned CCT banks on the heat load. It was stated that the extreme increases in the heating rate were 30% and 20% for staggered and in-line CCTs, respectively. The matching reductions in the pressure loss were 55 and 15%. Moawed [14] practically and numerically presented the hydrothermal performance of an airflow across inline isofluxed SCT bank. The authors considered a single SCT instead of an CCT; not pairs. Numerous transversal pitch ratios and attack angles of the SCTs were studied. In another work, Ibrahiem and Elsayed [15] extended the tests with staggered configuration. Wang et al. [16] simulated the turbulent flow attributes through a staggered CCT bank. The visualization supplied a good description for the vortex shedding. Khan et al. [17, 18] presented analytical analyses for the heat exchange

rate from tube bundle of inline and staggered arrangements. Furthermore, Khan et al. [19] applied an entropy minimization method to examine the thermodynamic losses caused by heat exchange and pressure loss for air flow across CCT banks. Zhang et al. [20] experimentally investigated the influence of incorporating vortex generators in finned isothermal CCT bundle of aligned and staggered arrangements. The results stated that vortex generators equipped to fin surfaces have tinyeffects on heat transfer performance.

Odabaee and Hooman [21] presented numerical simulations on the heat exchange from a metal foam enveloped CCT bundle. Another practical study was performed by Bayat et al. [22] using cam shaped staggered CCT bundle. The authors reported that the flow resistance was 92-93% lesser than CCT bank.Gong et al. [23] presented simulations of the heat load and flow contours around CCTs integrated with fins/vortex generators. Kiatpachai et al. [24] experimentally tested the result of employing spiral fin at different pitches on hydrothermal response of cross flow heat exchanger of two rows. Abdel-Rehim [25] numerically studied the hydrothermal behaviour of air across a staggered CCT bank. Zhang et al. [26] numerically and practically examined the hydrothermal attributes of an oblique airflow across isofluxed tube bank with different impinging angles. In their numerical analyses Bacellar et al. [27] considered the effect of operating condition of air flow across isothermal tube bundle of small diameters between 0.5 to 2 mm. Lavasani and Bayat [28] simulated the thermal and flow attributes of water based nanofluid across cam shaped and CCT bundle. Compared to CCT, it was reported that flow friction was reduced by 71% and 74% for in-line and staggered arrangement, respectively, by using cam shape.

Toolthaisong and Kasayapanand [29] tested the heat exchange from staggered flatten tube bundle in cross flow. Several attack angles of the flatten tubes were investigated. The results assured that the angle of attack technique could boost the overall heat exchange with higher pressure drop. Hu et al. [30] simulated the thermal attributes of airflow across finned CCT bank with/without winglet vortex generator of three different configurations. Li et al. [31] conducted practical tests using staggered twisted oval shape instead of CCTs as a tube bundle. Deng et al. [32] presented simulations for the particles flow and velocity patterns when flowing across staggered bundle of CCTs in moving bed. Zheng et al. [33] simulated the ash deposition and heat exchange behaviour on staggered CCTs bundles. From the presented survey, numerous studies were practically/numerically accomplished aiming to boost the hydrothermal attributes of tube banks. It is clear most of the works concentrated on applying fins/vortex generators. Here, it is aimed to test another approach of passive techniques which do not consume any direct power during life[34-40]. The existing study experimentally judges the heat load/flow resistance associated with an airflow crossing staggered pairs of CCTs/SCTs at different airflow rates. During the runs, several spaces between the tubes' bases and numerous spaces between the tubes in the longitudinal/transversal orders are experienced. An outline of an SCT is supplied in Fig. 1, in which the space between the bases is expressed in a nondimensional index (gap ratio; λ), assessed as follows;

$$\lambda = \frac{S_B}{d_{t,o}} \quad (1)$$

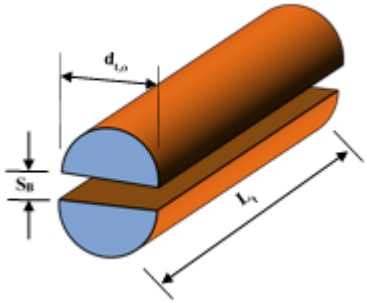

Fig. 1 Geometry of pair of SCTs.

2. Practical Apparatus

The test bench carried out in the present work includes two loops; hot and cold. The airflow loop consists of an open circulating stream, which includes a suction type air blower (5 hp), an air valve control unit, an orifice plate gauge, a transmission duct, pressure transmitters, a test section with different tube configurations, a tunnel inlet, a straightener, and an electric heater. The cooling water loop consists of a closed stream, which includes a chiller unit, a pump, ball valves, a flow meter, an inlet header, a test tube bundle, an outlet header and connecting tubes. Figs. 2 and 3 show schematic diagrams of the test device. The built-in heater consists of two stages, with a capacity of 6 kW, and they are controlled through a pre-set thermostat. The main tunnel is made of galvanized steel and is shaped into a rectangle with a width of 950 mm, a height of 250 mm and a length of 3500 mm. The outside of the tunnel is wrapped with glass wool. After leaving the inlet section, the air moves through the test section, which is positioned at 2000 mm from the air entry point. Two headers are installed in the vertical sides.

After leaving the main channel, the air reaches the metering channel through the transition section, which is formed as a converging unit. The metering channel consists of upstream PVC pipe, orifice plate and downstream PVC pipe. The orifice plate is designed according to the Miller standard [41]. Centrifugal type suction blower, driven by a 5 hp electric motor, is used to supply air to the pilot

machine at the required flow rate. The air flow rate is controlled via the damper. The water-cooling system includes a stainless-steel insulated tank with a capacity of 100 litters, in which heat is drawn through two refrigeration units with a cooling capacity of 20 kW. Besides, 3 hp centrifugal pump is employed to circulate the water. Water is pumped from the tank, flow meter, inlet head, circulated through pipes, outlet head, and then backed to the tank. Test tube packages consist of 17 CCTs or 34 SCTs; staggered arranged as five rows in the direction of flow while the odd and even rows having 3 and 4 tubes, respectively, as indicated in Fig. 4 and Table 1. The tested bundles are copper tubes having length of 1000 mm, 14.45 and 15.88 mm inner and outer diameters, respectively. Firstly, the CCT is cut longitudinally through a plasma cutter. Then the base of the SCT is formed as a copper sheet which is welded lengthwise.

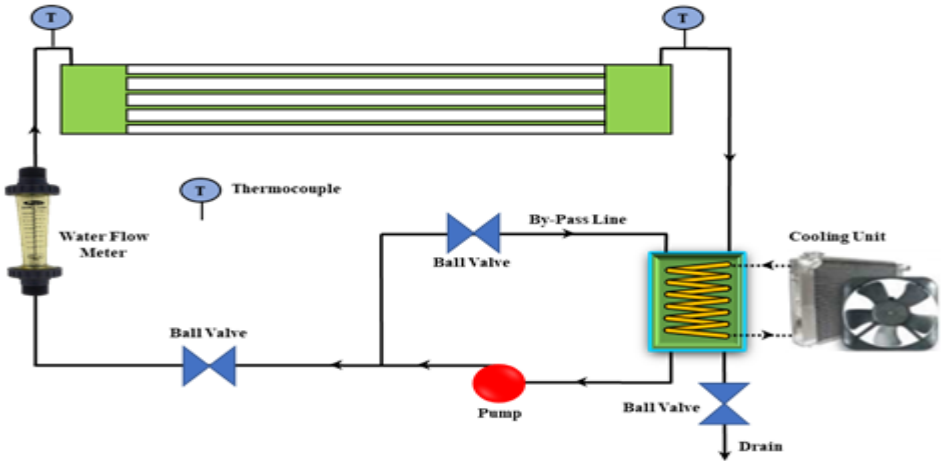

Fig. 2 An outline of the cooling loop.

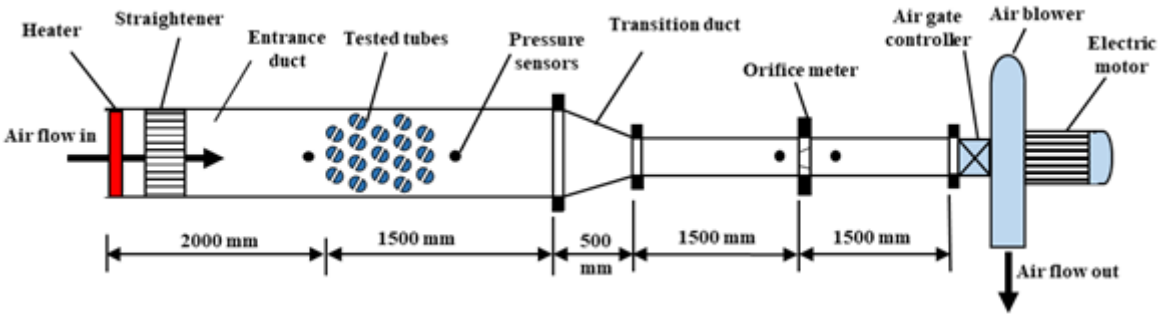

Fig. 3 An outline of the heating air loop.

Two tanks are integrated into the existing device, made of galvanized steel used to receive incoming water from/into the pipes. In total, 32 rectangular dies (Fig. 5) made of wooden panels with dimensions of 320 x 270 mm (wall thickness 4 mm) are located between the header and the nipples of the ductwork. The dies are drilled by a laser cutting machine to prepare holes of the same size and number of tubes as the test tube set. In addition, the inlet and outlet ports for the two heads are tubes of 100 and 50.8 mm long and inner diameter, respectively, welded to the heads. Moreover, the input and output ports are soldered to both heads. CCTs / SCTs are coupled to the two heads through dies, bearing in mind the sealing of the gap between the tubes and their holes in the die.

The air flowing rate is evaluated by estimating the pressure drop across the calibrated flow orifice plate via a digital pressure gauge (0.001-69 kPa pressure difference range, accuracy ± 1 Pa). Variable zone flow meter, range 10-100L / min, used to evaluate the flow rate of water, with an accuracy of ± 5% of the reading. Eight K-type thermocouples are used to estimate the temperatures of water and air entering and leaving the test section. Six of them are placed directly in the airflow stream; three at inlet and three at outlet of the test section. At each section, the three thermocouples are at positioned at distances from the top surface of the duct, which are equivalent to 16%, 32% and 50% of the duct hight. All thermocouples are connected via a switch specified with a digital indicator with an accuracy of 0.1°C

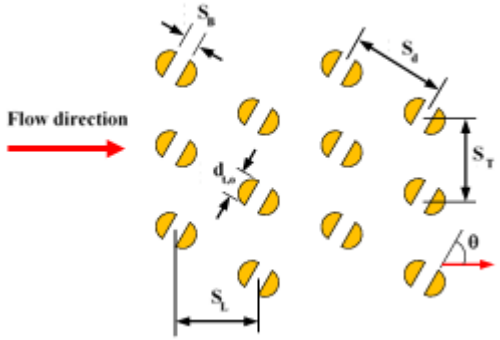

Fig. 4 Key dimensions of tested SCTs.

Fig. 5 Photo of the incorporated SCTs.

Table 1 Dimensions of the established tube banks.

No.	θ (°)	S_B (mm)	λ	S_T (mm)	τ	S_L (mm)	χ
CCTs							
1	———			31.75	2.0	31.75	2.0
SCTs							
2 to 16	45	2, 4, 6	0.126, 0.252, 0.378	31.75	2.0	31.75	2.0
				39.69	2.5		
				47.63	3.0	39.69	2.5
						47.63	3.0

3. Test Procedures

To start the tests, air blower, air gate control unit, orifice plate, transmission channel, test section, inlet duct, straightener, heater, tube bundle, heads, refrigeration unit, pump, water flow meter, thermocouple, and differential pressure transducer are connected. Moreover, the tubes are loaded and arranged in the duct according to the specified characteristics. The first step to collecting data from the system is to fill the cooling tank with water from the local water source. Then the blower, cooling unit, electric heater and pump are turned on. Fluid entry temperatures are regulated on both sides by regulating the temperatures of both the heater and the coolant tank through their respective thermostats. The water flow rate is adjusted by means of a flow meter and valve installation. While the air flow rate is controlled via an airflow retarder. A series of 112 experiments (7 airflow rates on 16 heat exchanger geometries shown in Table 1) is performed on the tested tube bank configurations. Through the test, it is assumed that steady state was recorded at a maximum change of 0.5°C within 25 min for each thermocouple.

Table 2: Operational conditions

Operational conditions	Range or Value
Air-side	
Airflow rate, m^3/s	0.285–1.677 $(1645 \leq Re_{o,max} \leq 12850)$
Inlet temperature, °C	50±1 ($Pr_o \approx 0.71$)
Water-side	
Total water flow rate, l/min	51.7 ($Re_i \approx 3272$)
Inlet temperature, °C	15 ($Pr_i \approx 7.94$)

4. Calculation methodologies

To get the properties of both fluids and to calculate the heat load of the water and air sides, firstly the mean temperature of the air at inlet and outlet are assessed. Then, the bulk temperature of the air and water are determined. These temperatures are also employed to assess the heat exchange of the water (Q_i) and of the air (Q_o). The deviation between the two loads is determined and compared to the average heat load. The maximum deviation for all experiments is 5.1%. using the average heat load and $\Delta T_{L.M}$ (calculate for counter flow), the $U_o A_{t,o}$ is calculated. Furthermore, the correction factor is judged [42], and the thermal resistances of fouling/conduction are ignored. So, the $U_o A_{t,o}$ is only function in convection resistance on both sides. It should be mentioned that $A_{t,o} = 17\pi d_{t,oi} L_t$ for CCTs, and $A_{t,o} = d_{t,o} L_t (17\pi + 34)$ for SCTs. The convection coefficient of the water is calculated by determining its $\overline{\mathrm{Nu}_i}$ via Gnielinski [43], Eq. (2), which is valid for $Re_i \geq 3000$. The Fanning friction factor in Eq. (3) is calculated according to Filonenko [44], through Eq. (3).

$$\overline{Nu_i} = \frac{\frac{f_i}{2}(Re_i - 1000)Pr_i}{1 + 12.7\sqrt{\frac{f_i}{2}}\left(Pr_i^{2/3} - 1\right)}\left[1 + \left(\frac{d_{t,h}}{L_t}\right)^{2/3}\right] \quad \textbf{(2)}$$

$$f_i = 0.25(1.82\, log\, Re_i - 1.64)^{-2} \quad \textbf{(3)}$$

The hydraulic diameter for the water side is $d_{t,i}$ for CCTs, while for SCTs, it is determined as $\pi d_{t,i}/(\pi + 2)$. Now, the $\overline{Nu_o}$ can be calculated based on the outer surface of the tubes. For staggered arrangement, the maximum velocity

of the cross flow ($u_{o,max}$) between the bundle is determined after comparing the ratio $2S_d/(S_T+d_{t,o})$[45], which is more than 1 for all runs. It is calculated based on the air velocity in the free duct (u_o). The measured ΔP_o is employed to assess the f_o as in Eq. (14) [9]. The followings are summary of the main used equations.

$$Q_i = \dot{m}_i Cp_i\left(T_{w,o} - T_{w,i}\right) \quad \textbf{(4)}$$

$$Q_o = \dot{m}_o Cp_o\left(T_{a,ave,i} - T_{a,ave,o}\right) \quad \textbf{(5)}$$

$$U_o A_{t,o} = \frac{Q_{ave}}{F\Delta T_{L.M}} \quad \textbf{(6)}$$

$$\Delta T_{L.M} = \frac{(\Delta T_i - \Delta T_o)}{\ln\left[\frac{\Delta T_i}{\Delta T_o}\right]} \quad \textbf{(7)}$$

$$\frac{1}{U_i A_{t,o}} = \frac{1}{\overline{h}_o A_{t,o}} + \frac{1}{\overline{h}_i A_{t,i}} \quad \textbf{(8)}$$

$$\overline{h}_i = \frac{\overline{Nu}_i . k_i}{d_{t,h}} \quad \textbf{(9)}$$

$$\overline{Nu}_o = \frac{\overline{h}_o d_{t,o}}{k_o} \quad \textbf{(10)}$$

$$u_{o,max} = \frac{u_o S_T}{S_T - d_{t,o}} \quad \textbf{(11)}$$

$$Re_{o,max} = \frac{u_{o,max} d_{t,o}}{\nu_o} \quad \textbf{(12)}$$

$$St_o = \frac{\overline{Nu}_o}{Re_{o,max}.Pr_o} \quad \textbf{(13)}$$

$$f_o = \frac{\Delta P_o}{2N_L \rho_o u_{o,max}^2} \quad \textbf{(14)}$$

5. Apparatus validation and data verification

The aforementioned steps and equations are incorporated to validate the experimental outputs of $\overline{Nu}_o$ and f_o. Their values are compared with Eq. (15) [4] and Eq. (16) [46]. These equations are valid for $10 \leq Re_{o,max} \leq 40000$. The comparisons are accomplished for CCT bundle presented in Table 1. It is seen in Fig. 6 that maximum documented differences are 7.1% and 6.1% for $\overline{Nu}_o$ and f_o, respectively.

$$\overline{Nu}_o = 0.33\, Re_{o,max}^{0.6} Pr_o^{1/3} \quad \textbf{(15)}$$

$$f_o = \left[0.25 + \frac{0.1175}{[(\tau-1)^{1.08}]}\right] Re_{o,max}^{-0.16} \quad \textbf{(16)}$$

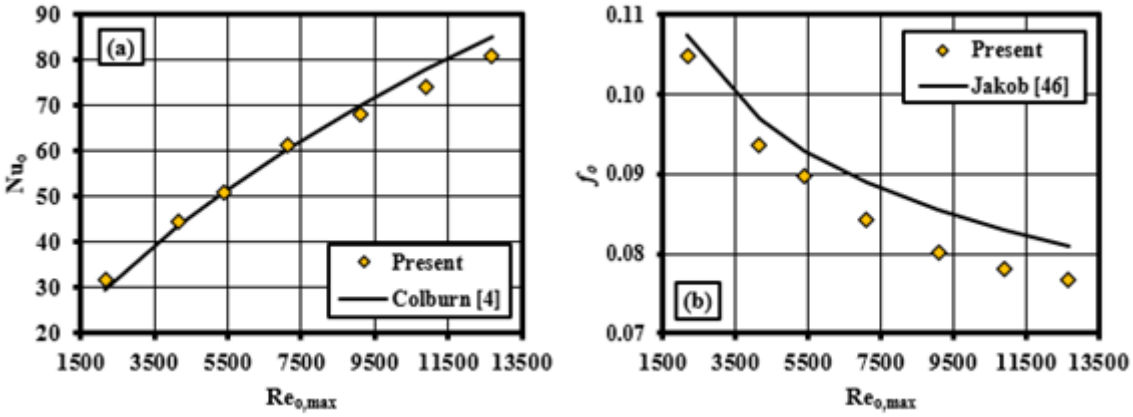

Fig. 6Outcomes of the comparisons; (a) $\overline{Nu}_o$, (b) f_o.

6. Results and discussions

6.1 Influence the space between the bases

In this section, three ratios of the spacing's ($0.126 \leq \lambda \leq 0.378$) for bases of the SCT banks are considered. Fig. 7 introduces the $\overline{Nu}_o$ and f_o for the examined spaces at different airflow rates at $\tau = \chi = 2.0$ and $\theta = 45°$ as a sample of the outputs. It is understandable that just splitting the tubes leads to augmenting the air-side heat transfer characteristics in addition to increasing the airflow pressure drop. These increases are enlarged by increasing the bases spaces. Compared with the CCT bank, the increases in $\overline{Nu}_o$ and f_o are 58.2% and 31.8%, respectively, at $\lambda = 0.126$. While by widening the SCT spacing ratio to 0.378, the corresponding percentage increases are magnified to be 63.7% and 39.8%, respectively.

One of the key reasons is that splitting the tube enlarges its contact area from ($\pi d_{t,o} L_t$) for CCT to be ($\pi d_{t,o} L_t + 2d_{t,o} L_t$) for pair of SCTs. In addition, increasing the space formed between the bases of semicircular tubes is accompanied with decreasing the flow gap between the tubes in different columns, which enlarges the flow mixing and turbulence level around the SCTs, and consequently breaks the boundary layers of the airflow. This results in increasing both the heat exchange rate and air-side flow resistance.

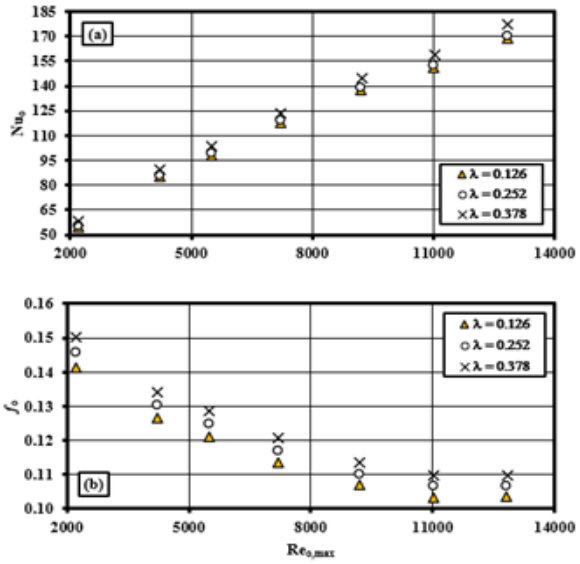

Fig. 7 The findings versus air-Reynolds number at different spaces between the bases (τ = χ = 2.0 and θ = 45°; (a) $\overline{Nu_o}$, (b) f_o.

6.2 Influence of transverse pitch ratio

In this section, experiments are accomplished with staggered arrangement at three different distances in the normal direction to the flow path (2 ≤ τ ≤ 3). The direction of the base is fixed at angle of 45°. A sample of the findings is outlined in Fig. 8 for χ = 2.0, θ = 45° and λ = 0.252. It is obvious that increasing the transversal pitch ratio of the tubes, reduces both $\overline{Nu_o}$ and f_o by 26.8% and 4.7%, respectively. The reduction in the heat transfer rates can be backed to that increasing the transversal pitch ratio of the tubes reduces the throttling for the airflow and produces weaker impingement with the later row of the tubes. Furthermore, this decreases the breaking of the air boundary layer, which consequently reduces the heat exchange rate besides reducing the flow pressure drop.

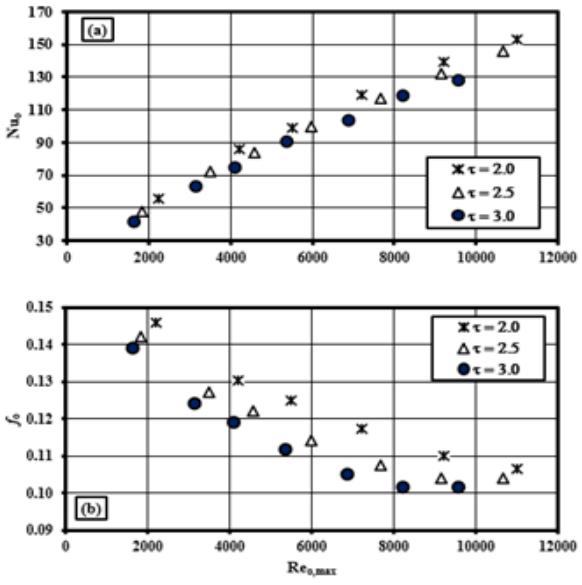

Fig. 8 Sample of the findings at three transversal pitch ratios χ=2.0,λ= 0.252,θ= 45°); (a) $\overline{Nu_o}$, (b) f_o.

6.3 Influence of longitudinal pitch ratio

Other tests are run at the staggered configuration to evaluate the influence of the pitch ratio in the flow direction; three different distances are considered (χ = 2, 2.5, 3). Also, the flow direction at the base is fixed at angle of 45°. A model of the results is declared in Fig. 9 for χ = 2.0, θ = 45° and λ = 0.252.

It is recorded that increasing the longitudinal pitch ratio of the tubes, from 2 to 3, reduces both $\overline{Nu_o}$ and f_o by 7.8% and 4.6%, respectively. These reductions can be due to increasing χ is accompanied by fewer rate and weaker impingement of the air molecules with the tubes. This reduces the disturbance around the tubes. Consequently, the mixings between air molecules and tube wall are dampened, which reduce the heat exchange rate besides decreasing the flow pressure decay.

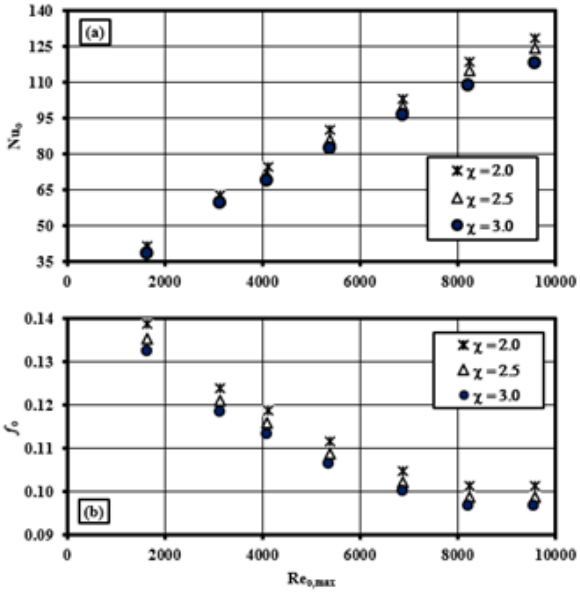

Fig. 9 Sample of the findings at three at different longitudinal pitch ratios (τ = 3, θ = 45° and λ = 0.252); (a) $\overline{Nu_o}$, (b) f_o.

6.4Thermal performance Index

In this study, the *TPI* is accessible by means of St_o and f_o ratios [35, 47] assessed with engaging SCTs and CCTs as heat transfer surfaces, as indicated in Eq. (17). Figs. 10 and 11 reports a sample of the average *TPIs* for different parameters.

$$TPI = \frac{St_{o,SCT}/St_{o,CCT}}{\left(f_{o,SCT}/f_{o,CCT}\right)^{1/3}} \qquad \textbf{(17)}$$

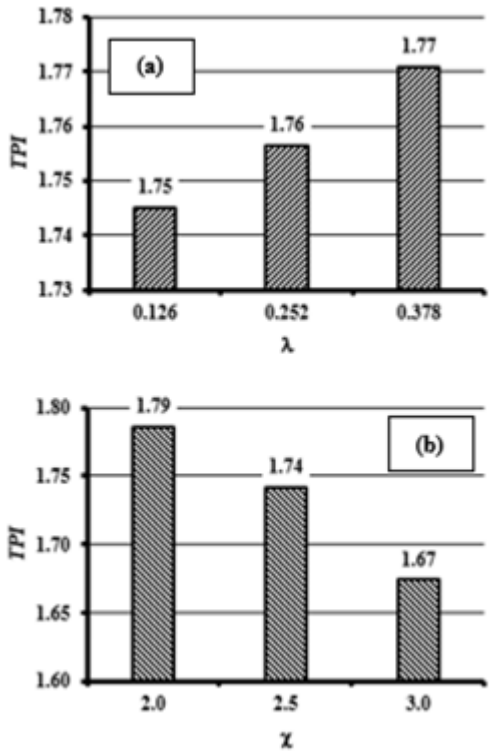

Fig. 10 The average *TPI* versus (a) SCTs' bases-gap, (b) transversal spacing ratio (τ=χ=2 &λ=0.378).

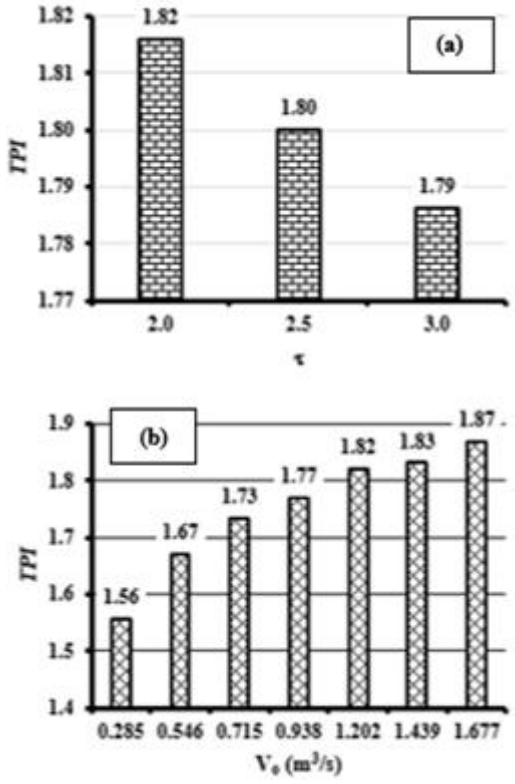

Fig. 11 The average *TPI* versus (a) longitudinal spacing ratio, (b) airflow rate (τ=χ=2 &λ=0.378).

It is clear that the *TPI* is slightly augmented by growing the gap between the SCTs' plane bases or reducing the transversal and/or longitudinal spacing ratios. Also, there is a significant increase in the *TPI* by speeding the airflow. Finally, the max. value of *TPI* is 1.98.

7. Summary

This study supplies tests on the hydrothermal characteristics of staggered CCT/SCT banks at a widespread range of air flowing rates crosswise the bundle. Through the runs, numerous gaps between SCTs-bases with different pitches in both longitudinal/transversal directions are tested. The results assure that:

- The SCT is an applicable passive heat transfer augmentation tool, but it increases the airflow resistance, simultaneously, when compared with using CCT.
- The $\overline{Nu}_o$ and f_o are enlarged by increasing the gap between the SCTs-bases and reducing the longitudinal and/or transversal pitch ratios of the tube bank.
- The *TPI* is slightly augmented by growing the gap between the SCTs' bases or reducing the transversal and/or longitudinal spacing ratios.
- There is an increase in the *TPI* by growing the airflow rate.
- The maximum informed value of *TPI* is 1.98.

References

[1] M.R. Salem, "Experimental investigation on the hydrothermal attributes of MWCNT/water nanofluid in the shell-side of shell and semi-circular tubes heat exchanger", Applied Thermal Engineering, vol. 176, Article no. 115438, 2020.

[2] T.L. Bergman, A.S. Lavine, F.P. Incropera and D.P. Dewitt, "Fundamentals of Heat and Mass Transfer", 7th edition, John Wiley & Sons, 2011.

[3] J.W. Baughn, M.J. Elderkin, A.A. McKillop, "Heat transfer from a single cylinder, cylinders in tandem, and cylinders in the entrance region of a tube bank with a uniform heat flux", Journal of Heat Transfer, vol. 108(2), pp. 386-391, 1986.

[4] A.P. Colburn, "A method of correlating forced convection heat transfer data and a comparison with fluid friction", Transactions of the American Institute of Chemical Engineers, vol. 29, pp. 174-210, 1933.

[5] O.L. Pierson, "Experimental investigation of the influence of tube arrangement on convection heat transfer and flow resistance in cross flow of gases over tube banks", Transactions of ASME, vol. 59, pp. 563-572, 1937.

[6] E.C. Huge, "Experimental investigation of effects of equipment size on convection heat transfer and flow resistance in cross flow of gases over tube banks", Transactions of ASME, vol. 59, pp. 573-581, 1937.

[7] G.A. Omohundro, O.P. Bergelin, A.P. Colburn, "Heat transfer and fluid friction during flow across banks of tubes", ASME Journal of Heat Transfer, vol. 71, pp. 27-34, 1949.

[8] A.J. Gram, C.O. Mackey, E.S. Monroe, "Convection heat transfer and pressure drop of air flowing across in-line tube banks: Part II - Correlation of data for ten-row-deep tube banks", Transactions of ASME, vol. 80, pp. 25-35, 1958.

[9] A. Zukauskas, "Heat transfer from tubes in cross flow", in J.P. Hartnett and T.F. Irvine, Jr., Eds., Advances in Heat Transfer, vol. 8, Academic Press, New York, 1972.

[10] J.C. Biery, "Prediction of heat transfer coefficients in gas flow normal to finned and smooth tube banks", Journal of Heat Transfer (ASME), vol. 103(4), pp. 705-714, 1981.

[11] G.P. Merker, H. Hanke, "Heat transfer and pressure drop on the shell-side of tube-banks having oval-shaped tubes", International Journal of Heat and Mass Transfer, vol. 29(12), pp. 1903-1909, 1986.

[12] N.H. Kim, B. Youn, R.L. Webb, "Air-side heat transfer and friction correlations for plain fin-and-tube heat exchangers with staggered tube arrangements", Journal of Heat Transfer, vol. 121(3), pp. 662-667, 1999.

[13] K. Torii, K.M. Kwak, K. Nishino, "Heat transfer enhancement accompanying pressure-loss reduction with winglet-type vortex generators for fin-tube heat exchangers", International Journal of Heat and Mass Transfer, vol. 45, pp. 3795-3801, 2002.

[14] M. Moawed, "Thermal performance of a cross flow heat exchanger with semi-circular tubes", ERJ Shoubra Faculty of Engineering, vol. 4, pp. 87-109, June 2005.

[15] E.Z. Ibrahiem, A.O. Elsayed, "Heat transfer performance of a semi-circular tube bank", Heat Transfer Research, vol. 46(6), pp. 563-576, 2015.

[16] Y.Q. Wang, P. Jackson, T.J. Phaneuf, "Turbulent Flow Through a Staggered Tube Bank", Journal of Thermophysics and Heat Transfer, vol. 20(4), pp. 738-747, 2006.

[17] W.A. Khan, J.R. Culham, M.M. Yovanovich, "Convection heat transfer from tube banks in crossflow: Analytical approach", International Journal of Heat and Mass Transfer, vol. 49 pp. 4831-4838, 2006.

[18] W.A. Khan, J.R. Culham, M.M. Yovanovich, "Analytical model for convection heat transfer from tube banks", Journal of Thermophysics and Heat Transfer, vol. 20(4), pp. 720-727, 2006.

[19] W.A. Khan, J.R. Culham, M.M. Yovanovich, "Optimal design of tube banks in crossflow using entropy generation minimization method", Journal of Thermophysics and Heat Transfer, vol. 21(2), pp. 372- 378, 2007.

[20] Y. Zhang, X. Wu, L. Wang, K. Song, Y. Dong, S. Liu, "Comparison of heat transfer performance of tube bank fin with mounted vortex generators to tube bank fin with punched vortex generators", Experimental Thermal and Fluid Science, vol. 33, pp. 58-66, 2008.

[21] M. Odabaee, K. Hooman, "Metal foam heat exchangers for heat transfer augmentation from a tube bank", Applied Thermal Engineering, vol. 36, pp. 456-463, 2012.

[22] H. Bayat, A.M. Lavasani, T. Maarefdoost, "Experimental study of thermal–hydraulic performance of cam-shaped tube bundle with staggered arrangement", Energy Conversion and Management, vol. 85, pp. 470-476, 2014.

[23] B. Gong, L. Wang, Z. Lin, "Heat transfer characteristics of a circular tube bank fin heat exchanger with fins punched curve rectangular vortex generators in the wake regions of the tubes", Applied Thermal Engineering, vol. 75, pp. 224-238, 2015.

[24] P. Kiatpachai, S. Pikulkajorn, S. Wongwises, "Air-side performance of serrated welded spiral fin-and-tube heat exchangers", International Journal of Heat and Mass Transfer, vol. 89, pp. 724-732, 2015.

[25] Z.S. Abdel-Rehim, "Heat transfer and turbulent fluid flow over staggered circular tube bank", Energy Sources, Part A: Recovery, Utilization, and Environmental Effects, vol. 37, pp. 164-173, 2015.

[26] L. Zhang, Y. Ouyang, Z. Zhang, S. Wang, "Oblique fluid flow and convective heat transfer across a tube bank under uniform wall heat flux boundary conditions", International Journal of Heat and Mass Transfer, vol. 91, pp. 1259–1272, 2015.

[27] D. Bacellar, V. Aute, Z. Huang, R. Radermacher, "Airside friction and heat transfer characteristics for staggered tube bundle in crossflow configuration with diameters from 0.5 mm to 2.0 mm", International Journal of Heat and Mass Transfer, vol. 98, pp. 448-454, 2016.

[28] A.M. Lavasani, H. Bayat, "Numerical study of pressure drop and heat transfer from circular and cam-shaped tube bank in cross-flow of nanofluid", Energy Conversion and Management, vol. 129, pp. 319-328, 2016.

[29] S. Toolthaisong, N. Kasayapanand, "Heat transfer enhancement in a cross-flow heat exchanger with modified air angles of attack", Journal of Energy Engineering, vol. 142(3), article no. 04015044, pp. 1-,6 2016.

[30] W. Hu, L. Wang, Y. Guan, W. Hu, "The effect of shape of winglet vortex generator on the thermal–hydrodynamic performance of a circular tube bank fin heat exchanger", Heat Mass Transfer, vol. 53, pp. 2961-2973, 2017.

[31] X. Li, D. Zhu, J. Sun, X. Mo, S. Liu, "Heat transfer and pressure drop for twisted oval tube bundles with staggered layout in crossflow of air", Applied Thermal Engineering, vol. 148, pp. 1092-1098, 2019.

[32] S. Deng, Z. Wen, G. Lou, D. Zhang, F. Su, X. Liu, R. Dou, "Process of particles flow across staggered tubes in moving bed", Chemical Engineering Science, vol. 217, article no. 115507, 2020.

[33] Z. Zheng, W. Yang, Y. Cai, Q. Wang, G. Zeng, "Dynamic simulation on ash deposition and heat transfer behavior on a staggered tube bundle under high-temperature conditions", Energy, vol. 190, article no. 116390, 2020.

[34] M.R. Salem, K.M. Elshazly, R.Y. Sakr, R.K. Ali, Experimental study on convective heat transfer and pressure drop of water-based nanofluid inside shell and coil heat exchanger, PhD dissertation, Faculty of Engineering at Shoubra, Benha University, 2014.

[35] M.R. Salem, M.B. Eltoukhey, R.K. Ali, K.M. Elshazly, "Experimental investigation on the hydrothermal performance of a double-pipe heat exchanger using helical tape insert", International Journal of Thermal Sciences, vol. 124, pp. 496-507, 2018.

[36] K.M. Elshazly, R.Y. Sakr, R.K. Ali, M.R. Salem, "Effect of γ-Al2O3/Water Nanofluid on the Thermal Performance of Shell and Coil Heat Exchanger with Different Coil Torsions", Heat and Mass Transfer, vol. 53 (6), 1893-1903, 2017.

[37] M.R. Salem, "Performance enhancement of a vapor compression refrigeration system using R134a/MWCNT-oil mixture and liquid-suction heat exchanger equipped with twisted tape turbulator", International Journal of Refrigeration, vol. 120, 357-369, 2020.

[38] S.M. Elshamy, M.T. Abdelghany, M.R. Salem, O.E. Abdellatif, "Based Al_2O_3 Nanofluid Including Diverse Coil Geometries: An Experimental Study", Journal of Nanofluids, vol. 9 (1), 13-23, 2020.

[39] M.R. Salem, H.A. El-Gammal, A.A. Abd-Elaziz, K.M. Elshazly, "Study of the performance of a vapor compression refrigeration system using conically coiled tube-in-tube evaporator and condenser", International Journal of Refrigeration, vol. 99, 393-407, 2019

[40] H.A. Refaey, E. Specht, M.R. Salem, "Influence of Fuel Distribution and Heat Transfer on Energy Consumption in Tunnel Kilns", International Journal of Advances in Engineering & Technology (IJAET), vol. 8(3), 281-293, 2015.

[41] R.W. Miller, "Flow measurement engineering handbook", 3rd edition, New York: McGraw-Hill, 2000.

[42] R.K. Shah, D.P. Sekulić, "Fundamentals of heat exchanger design", 6th edition, Hoboken, NJ: John Wiley & Sons, p. 189, 2003.

[43] V. Gnielinski, "New equations for heat and mass transfer in turbulent pipe and channel flow", International Chemical Engineering, vol. 16, pp. 359-368, 1976.

[44] G.K. Filonenko, "Hydraulic resistance of pipes (HydraulischerWiderstand von Rohrleitungen)," Teploenergetika, vol. 1(4), pp. 40-44, 1954.

[45] F.W. Dittus, L.M.K. Boelter, "Heat transfer in automobile radiators of the tubular type", University of California Publications in Engineering, vol. 2, p. 433, 1930.

[46] M. Jakob, "Heat transfer and flow resistance in cross flow of gases over tube banks", Trans. ASME, vol. 60, p. 384, 1938.

[47] H.H. Al-Kayiem, A. Bin Ekhwan, L.N. Muhi, "Augmentation of ribs turbulators height on the hydrothermal performance of double pipe heat exchanger", Journal of Engineering Science and Technology, vol. 12(2), pp. 548-563, 2017.

Appendix A: Uncertainty Estimation

According to the manufacturer, the uncertainty in the CCT diameters is ±0.01 mm. Moreover, the uncertainty in the spacing between the SCT-bases and pitches is ± 0.01 mm. Furthermore, the uncertainty in the other measured dimensions is assumed to be ± 0.5 mm. Therefore, the maximum uncertainties in the spacing ratios, distances and areas are;

$$\frac{\omega_\lambda}{\lambda} = \pm\sqrt{\left(\frac{\omega_{S_B}}{S_B}\right)^2 + \left(\frac{-\omega_{d_{t,o}}}{d_{t,o}}\right)^2} = \pm 0.504\% \quad \textbf{(18)}$$

$$\frac{\omega_\tau}{\tau} = \frac{\omega_\chi}{\chi} = \pm\sqrt{\left(\frac{\omega_{S_T}}{S_T}\right)^2 + \left(\frac{-\omega_{d_{t,o}}}{d_{t,o}}\right)^2} = \pm 0.076\% \quad \textbf{(19)}$$

$$\omega_{S_T - d_{t,o}} = \pm\sqrt{\left(\omega_{S_T}\right)^2 + \left(-\omega_{d_{t,o}}\right)^2} == \pm 0.014 \text{ mm} \quad \textbf{(20)}$$

$$\frac{\omega_{A_{t,o}}}{A_{t,o}} = \pm\sqrt{\left(\frac{\omega_{d_{t,o}}}{d_{t,o}}\right)^2 + \left(\frac{\omega_{L_t}}{L_t}\right)^2} = \pm 0.082\% \quad \textbf{(21)}$$

$$\frac{\omega_{A_{t,i}}}{A_{t,i}} = \pm\sqrt{\left(\frac{\omega_{d_{t,i}}}{d_{t,i}}\right)^2 + \left(\frac{\omega_{L_t}}{L_t}\right)^2} = \pm 0.087\% \quad \textbf{(22)}$$

$$\frac{\omega_{A_{bore}}}{A_{bore}} = \pm\sqrt{\left(\frac{\omega_W}{W}\right)^2 + \left(\frac{\omega_H}{H}\right)^2} = \pm 0.21\% \quad \textbf{(23)}$$

$$\frac{\omega_{A_{orifice}}}{A_{orifice}} = \pm\sqrt{\left(\frac{2\omega_{d_{orifice}}}{d_{orifice}}\right)^2} = \pm 0.984\% \quad \textbf{(24)}$$

The uncertainties in the temperature readings and temperature differences are;

$$\omega_{\Delta T_w} = \pm\sqrt{\left(\omega_{T_{w,o}}\right)^2 + \left(-\omega_{T_{w,i}}\right)^2} = \pm 0.71℃ \quad \textbf{(25)}$$

$$\omega_{\Delta T_a} = \pm\sqrt{\left(\frac{\partial \Delta T_a}{\partial T_{a,i}}\omega_{T_{a,i}}\right)^2 + \left(\frac{\partial \Delta T_a}{\partial T_{a,o}}\omega_{T_{a,o}}\right)^2} = \pm 0.06℃ \quad \textbf{(26)}$$

$$\omega_{\Delta T_i} = \omega_{\Delta T_o} = \pm\sqrt{\left(\frac{\partial \Delta T_i}{\partial T_{a,ave,i}}\omega_{T_{a,ave,i}}\right)^2 + \left(\frac{\partial \Delta T_i}{\partial T_{w,o}}\omega_{T_{w,o}}\right)^2} \cong \pm 0.5℃ \quad \textbf{(27)}$$

$$\omega_{\Delta T_{L.M}} = \pm\frac{\omega_T\sqrt{2}}{\ln\left[\frac{\Delta T_i}{\Delta T_o}\right]}\sqrt{2 - 2\Delta T_{L.M}\left(\frac{1}{\Delta T_i} + \frac{1}{\Delta T_o}\right) + \Delta T_{L.M}^2\left(\frac{1}{\Delta T_i^2} + \frac{1}{\Delta T_o^2}\right)} \quad \textbf{(28)}$$

The uncertainties applied to the thermal properties of the working fluids are assumed to be ±0.1%. The uncertainties associated with estimating the tank volume and collecting time are ± 0.01 litre and ± 1 s, respectively. The

measurement is taken for a flow rate of 50 l/min. Therefore, the uncertainty is found to be 1.67% of the full scale, as follows;

$$\omega_{\dot{V}_w} = \pm\sqrt{\left(\frac{\partial \dot{V}_w}{\partial V_w}\omega_{V_w}\right)^2 + \left(\frac{\partial \dot{V}_w}{\partial t}\omega_t\right)^2} = \pm\sqrt{\left(\frac{1}{t}\omega_{V_w}\right)^2 + \left(\frac{-V}{t^2}\omega_t\right)^2} \quad (29)$$

The uncertainty in water mass flow rate and Reynolds number are obtained as follows;

$$\frac{\omega_{\dot{m}_w}}{\dot{m}_w} = \pm\sqrt{\left(\frac{\omega_{\rho_w}}{\rho_w}\right)^2 + \left(\frac{\omega_{\dot{V}_w}}{\dot{V}_w}\right)^2} = \pm 1.67\% \quad (30)$$

$$\frac{\omega_{Re_i}}{Re_i} = \pm\sqrt{\left(\frac{\omega_{\dot{m}_w}}{\dot{m}_w}\right)^2 + \left(\frac{\omega_{d_{t,h}}}{d_{t,h}}\right)^2 + \left(\frac{\omega_{\mu_i}}{\mu_i}\right)^2} \cong \pm 1.67\% \quad (31)$$

The maximum uncertainties in the air velocities, Reynolds number and flow rate are calculated as follows;

$$\frac{\omega_{u_o}}{u_o} = \pm\sqrt{\left(\frac{0.7566\,\omega_{\Delta H_o}}{\Delta H_o}\right)^2 + \left(\frac{\omega_{A_{bore}}}{A_{bore}}\right)^2 + \left(\frac{\omega_{A_{orifice}}}{A_{orifice}}\right)^2} \cong \pm 4.29\% \quad (32)$$

$$\frac{\omega_{u_{o,max}}}{u_{o,max}} = \pm\sqrt{\left(\frac{\omega_{u_o}}{u_o}\right)^2 + \left(\frac{\omega_{S_T}}{S_T}\right)^2 + \left(\frac{\omega_{S_T - d_{t,o}}}{S_T - d_{t,o}}\right)^2} \cong \pm 4.29\% \quad (33)$$

$$\frac{\omega_{Re_{o,max}}}{Re_{o,max}} = \pm\sqrt{\left(\frac{\omega_{u_{o,max}}}{u_{o,max}}\right)^2 + \left(\frac{\omega_{d_{t,o}}}{d_{t,o}}\right)^2 + \left(\frac{\omega_{\nu_o}}{\nu_o}\right)^2} \cong \pm 4.29\% \quad (34)$$

$$\frac{\omega_{\dot{V}_o}}{\dot{V}_o} = \pm\frac{0.7566\,\omega_{\Delta H_{orifice}}}{\omega_{\Delta H_{orifice}}} = \pm 0.32\%\ (\text{max. value}) \quad (35)$$

$$\frac{\omega_{\dot{m}_o}}{\dot{m}_o} = \pm\sqrt{\left(\frac{\omega_{\dot{V}_o}}{\dot{V}_o}\right)^2 + \left(\frac{\omega_{\rho_o}}{\rho_o}\right)^2} = \pm 0.33\%\ (\text{max. value}) \quad (36)$$

The maximum uncertainties in the heat transfer loads and other performance parameters are evaluated as follows;

$$\frac{\omega_{Q_o}}{Q_o} = \pm\sqrt{\left(\frac{\omega_{\dot{m}_o}}{\dot{m}_o}\right)^2 + \left(\frac{\omega_{Cp_o}}{Cp_o}\right)^2 + \left(\frac{\omega_{\Delta T_a}}{\Delta T_a}\right)^2} = \pm 4.04\%\ (\text{max. value}) \quad (37)$$

$$\frac{\omega_{Q_i}}{Q_i} = \pm\sqrt{\left(\frac{\omega_{\dot{m}_i}}{\dot{m}_i}\right)^2 + \left(\frac{\omega_{Cp_i}}{Cp_i}\right)^2 + \left(\frac{\omega_{\Delta T_w}}{\Delta T_w}\right)^2} = \pm 1.69\%\ (\text{max. value}) \quad (38)$$

$$\omega_{Q_{ave}} = \pm\frac{1}{2}\sqrt{(\omega_{Q_o})^2 + (\omega_{Q_i})^2} = \pm 2.19\%\ (\text{max. value}) \quad (39)$$

$$\frac{\omega_{U_o}}{U_o} = \pm\sqrt{\left(\frac{\omega_{Q_{ave}}}{Q_{ave}}\right)^2 + \left(\frac{-\omega_{A_{t,o}}}{A_{t,o}}\right)^2 + \left(\frac{-\omega_{\Delta T_{L,M}}}{\Delta T_{L,M}}\right)^2} = \pm 2.26\%\ (\text{max. value}) \quad (40)$$

$$\frac{\omega_{\overline{Nu}_i}}{\overline{Nu}_i} = \pm\sqrt{\left(\frac{0.8\,\omega_{Re_i}}{Re_i}\right)^2 + \left(\frac{0.4\,\omega_{Pr_i}}{Pr_i}\right)^2} \cong \pm 1.34\%\ (\text{max. value}) \quad (41)$$

$$\frac{\omega_{\overline{h}_i}}{\overline{h}_i} = \pm\sqrt{\left(\frac{\omega_{\overline{Nu}_i}}{\overline{Nu}_i}\right)^2 + \left(\frac{\omega_{k_i}}{k_i}\right)^2 + \left(\frac{-\omega_{d_{t,h}}}{d_{t,h}}\right)^2} \cong \pm 1.35\%\ (\text{max. value}) \quad (42)$$

$$\omega_{\overline{h}_o} = \pm\sqrt{\left(\frac{\partial \overline{h}_o}{\partial U_o}\omega_{U_o}\right)^2 + \left(\frac{\partial \overline{h}_o}{\partial A_{t,o}}\omega_{A_{t,o}}\right)^2 + \left(\frac{\partial \overline{h}_o}{\partial A_{t,i}}\omega_{A_{t,i}}\right)^2 + \left(\frac{\partial \overline{h}_o}{\partial \overline{h}_i}\omega_{\overline{h}_i}\right)^2} \cong \pm 4.66\%\ (\text{max.}) \quad (43)$$

$$\frac{\omega_{\overline{Nu}_o}}{\overline{Nu}_o} = \pm\sqrt{\left(\frac{\omega_{\overline{h}_o}}{\overline{h}_o}\right)^2 + \left(\frac{\omega_{d_{t,o}}}{d_{t,o}}\right)^2 + \left(\frac{-\omega_{k_o}}{k_o}\right)^2} \cong \pm 4.67\%\ (\text{max. value}) \quad (44)$$

$$\frac{\omega_{\overline{Nu}_o}}{\overline{Nu}_o} = \pm\sqrt{\left(\frac{\omega_{\overline{h}_o}}{\overline{h}_o}\right)^2 + \left(\frac{\omega_{d_{t,o}}}{d_{t,o}}\right)^2 + \left(\frac{-\omega_{k_o}}{k_o}\right)^2} \cong \pm 4.67\%\ (\text{max. value}) \quad (45)$$

$$\frac{\omega_{St_o}}{St_o} = \pm\sqrt{\left(\frac{\omega_{\overline{Nu}_o}}{\overline{Nu}_o}\right)^2 + \left(\frac{\omega_{Re_{o,max}}}{Re_{o,max}}\right)^2 + \left(\frac{-\omega_{Pr_o}}{Pr_o}\right)^2} \cong \pm 6.34\%\ (\text{max. value}) \quad (46)$$

$$\frac{\omega_{f_o}}{f_o} = \pm\sqrt{\left(\frac{\omega_{\Delta P_o}}{\Delta P_o}\right)^2 + \left(\frac{\omega_{\rho_o}}{\rho_o}\right)^2 + \left(\frac{-2\omega_{u_{o,max}}}{u_{o,max}}\right)^2} \cong \pm 5.8\%\ (\text{max. value}) \quad (47)$$

$$\frac{\omega_{TPI}}{TPI} = \pm\sqrt{\left(\frac{\omega_{St_{o,SCT}}}{St_{o,SCT}}\right)^2 + \left(\frac{\omega_{St_{o,CCT}}}{St_{o,CCT}}\right)^2 + \left(\frac{\frac{1}{3}\omega_{f_{o,SCT}}}{f_{o,SCT}}\right)^2 + \left(\frac{\frac{1}{3}\omega_{f_{o,CCT}}}{f_{o,CCT}}\right)^2} \cong \pm 6.71\%\ (\text{max.}) \quad (48)$$

Nomenclatures

A	Area, m^2
Cp	Specific heat, $J/kg.℃$
d	Diameter, m
f	Fanning friction factor
h	Convection heat transfer coefficient, $W/m^2.℃$
k	Thermal conductivity, $W/m.℃$
L	Length, m
$\dot{m}$	Mass flow rate, kg/s
P	Pressure, Pa
Q	Heat transfer rate, W
S	Gap between the bases of two adjacent SCTs, m
T	Temperature, ℃ or K
u	Velocity, m/s
$\dot{V}$	Volume flow rate, m^3/s

Dimensionless groups

$\overline{Nu}$	Average Nusselt number
Pr	Prandtl number
Re	Reynolds number
St	Stanton number

Greek letters

Δ	Differential
π	A mathematical constant ≅ 3.1416
λ	Base gap ratio
ρ	Density, kg/m^3
θ	Attack angle, °

Superscripts and subscripts

ave	Average
b	Base
c	Cross-sectional
cir	Circular
h	Hydraulic
i	Inner or inlet or internal
LM	Logarithmic Mean
m	Mean
max	Maximum
o	Out or outer
s	Surface
t	Tube

Acronyms and abbreviations

CCT	Complete Circular Tube
SCT	Semi-Circular Tube
TPI	Thermal Performance Index